Optimization of 3D-Printed Patterns Parameters and Two-Stage Burnout Process for Defect Reduction in Propeller Blades Investment Casting Shell Mold

Zolkarnain Marjom*., Ahmad Syazani Ahmad Moktar., Mohamad Ridzuan Mohamad Kamal

Facuty of Industrial & Manufacturing Technology & Engineering, Universiti Teknikal Malaysia Melaka

DOI: https://doi.org/10.47772/IJRISS.2025.91200055

Received: 10 December 2025; Accepted: 17 December 2025; Published: 31 December 2025

ABSTRACT

This study investigates the optimization of 3D-printed investment casting patterns and two-stage burnout parameters to minimize defects in propeller blade manufacturing. A full factorial design of experiments (2^4) was implemented to analyze the effects of four fused deposition modeling (FDM) parameters—shell thickness, infill density, layer height, and internal pattern structure—on burnout performance. Thirty-two PLA patterns were fabricated and evaluated through a two-stage burnout process: Stage 1 (200–350 °C) assessed air permeability, while Stage 2 (up to 650 °C) examined surface integrity using dye penetrant testing and visual crack inspection. Statistical analysis using GLM ANOVA revealed that air permeability exhibited no significant main effects but was influenced by higher-order interactions, notably Infill× Shell× Pattern ($F = 5.067$, $p = 0.03879$) and Layer× Shell× Pattern ($F = 6.975$, $p = 0.01779$). Dye penetrant indications were dominated by shell thickness ($F = 2135.9$, $p \approx 1.84e^{-}18$), with layer height and multiple interactions also significant. Visual cracking was strongly associated with shell thickness (Fisher exact $p = 0.00245$), with 1 mm shells reducing defects compared to 2 mm. The findings underscore that shell thickness is the primary factor for Stage 2 defect mitigation, while Stage 1 optimization requires joint tuning of shell, infill, and pattern parameters. The proposed two-stage burnout workflow enables early identification of critical factor combinations, offering a robust approach for improving dimensional integrity and surface quality in additively manufactured investment casting applications.

Keywords: Additive Manufacturing; Investment Casting; Two-Stage Burnout; DOE; ANOVA; Air Permeability; Dye Penetrant; Cracking.

INTRODUCTION

Investment casting (IC) is widely employed for manufacturing components requiring high dimensional accuracy and intricate geometries, particularly in aerospace and marine applications [1, 20]. Conventional IC processes rely on wax patterns, which require tooling and limit design flexibility [3]. The integration of additive manufacturing (AM) technologies has enabled the production of expendable patterns directly from digital models, significantly reducing lead time and cost [4, 7].

3D printing with Fused deposition modeling (FDM) technology is among the most accessible AM techniques for producing polymer-based investment casting patterns due to its low cost and material availability [5,13]. Polylactic acid (PLA) is commonly used; however, its thermal degradation behaviour differs from wax, resulting in complex gas evolution during burnout [11]. Insufficient gas evacuation may lead to shell cracking and surface defects, especially in enclosed geometries such as propeller blades [15].

Previous studies often evaluate burnout-related defects only after complete pattern removal [6, 8]. Such approaches overlook the importance of early-stage gas evacuation behaviour, which significantly influences shell integrity during subsequent high-temperature exposure. Furthermore, the combined effects of infill density, internal pattern structure, and shell thickness on permeability and cracking behaviour have not been systematically quantified using statistical design methods [9].

To address these gaps, this study adopts a two-stage burnout strategy that separates air permeability evaluation from final crack assessment. A full factorial DOE is employed to statistically analyse the influence of key FDM parameters on both responses, enabling improved understanding and optimisation of additively manufactured investment casting patterns.

METHODOLOGY

The creation of the propeller blade begins with design using CATIA software. The model is exported as an STL file, imported into Ultimaker Cura software, and printed using PLA filament.

A full factorial design of experiment (2^4) was adopted to evaluate the effects of four FDM process parameters: infill density (10% and 20%), layer height (0.10 mm and 0.15 mm), shell thickness (1 mm and 2 mm), and internal pattern structure (gyroid and concentric). Sixteen experimental runs were conducted using PLA patterns fabricated via FDM with two replicates (n = 32).

Ceramic shells were prepared using a conventional slurry dipping process as described in the investment casting literature [1,3]. Burnout was performed in two stages. Stage 1 involved partial burnout between 200 and 350 °C to initiate polymer degradation while maintaining shell integrity. Air permeability tests were conducted. Stage 2 extended heating to 650 °C to ensure complete pattern removal, followed by visual crack inspection and dye penetrant testing per ASTM E1417. **Figure 1** shows Air Permeability test & Dye Penetration Test (NDT).

Figure 1. Air Permeability Test & Dye Penetration Test (NDT) Sample

RESULTS AND DISCUSSION

A balanced 2^4 full factorial design with two replicates (n = 32) was analysed for four factors: Infill (10%, 20%), Layer height (0.10, 0.15 mm), Shell thickness (1, 2 mm), and Pattern (Gyroid, Concentric). Responses were: Air Permeability (after Stage-1 burnout 200–350 °C), Dye Penetrant indication (after Stage-2 burnout up to 650 °C), and Visual Crack (binary).

Analyses employed GLM ANOVA (Type II) consistent with Minitab practice for balanced factorials. Residual diagnostics were performed; exact tests were used for the binary cracking response due to separation at 2 mm shell.

DOE Factors and Levels

Table 1 shows factors and levels: Infill (10%, 20%), Layer height (0.10 mm, 0.15 mm), Shell thickness (1 mm, 2 mm), Pattern (Gyroid, Concentric).

Table 1. Full factorial DOE matrix with run order and factor settings.

	Parameters				Responds		
Run	**Infill density**	**Layer height**	**Shell Thickness**	**Pattern Type**	**Visual Crack**	**AirPerm**	**Dye**
1	10	0.15	1	Gyroid	0	0.0184	6.45
2	10	0.15	1	Gyroid	1	0.0196	6.95
3	10	0.1	2	Gyroid	1	0.019	23.12
4	10	0.1	2	Gyroid	1	0.0204	24.7
5	10	0.1	1	Gyroid	0	0.0191	8.94
6	10	0.1	1	Gyroid	1	0.0205	9.6
7	20	0.15	2	Gyroid	1	0.0193	15.37
8	20	0.15	2	Gyroid	1	0.0208	16.6
9	20	0.15	1	Gyroid	1	0.0198	12.55
10	20	0.15	1	Gyroid	1	0.0212	13.5
11	10	0.15	2	Gyroid	1	0.0207	27.33
12	10	0.15	2	Gyroid	1	0.0222	29
13	10	0.15	2	Concentric	1	0.0189	29.74
14	10	0.15	2	Concentric	1	0.0203	31.6
15	10	0.1	1	Concentric	0	0.0178	0
16	10	0.1	1	Concentric	0	0.0189	0.4
17	20	0.15	2	Concentric	1	0.0196	11.62
18	20	0.15	2	Concentric	1	0.021	12.5
19	20	0.15	1	Concentric	1	0.0193	17.84
20	20	0.15	1	Concentric	1	0.0208	19
21	20	0.1	1	Gyroid	0	0.0201	8.44
22	20	0.1	1	Gyroid	1	0.0216	9.2
23	20	0.1	2	Gyroid	1	0.0189	11.55
24	20	0.1	2	Gyroid	1	0.0203	12.4

25	20	0.1	1	Concentric	0	0.0189	6.65
26	20	0.1	1	Concentric	1	0.0203	7.2
27	10	0.15	1	Concentric	0	0.02	0
28	10	0.15	1	Concentric	0	0.0215	0.5
29	10	0.1	2	Concentric	1	0.0188	20.14
30	10	0.1	2	Concentric	1	0.0202	21.5
31	20	0.1	2	Concentric	1	0.0209	28.54
32	20	0.1	2	Concentric	1	0.0224	30.7

Air Permeability (Stage-1, 200–350 °C)

Mean air permeability was slightly higher at the "upper" levels of each factor: 20% infill (0.02033 vs 0.01977), 0.15 mm layer height (0.02021 vs 0.01988), 2 mm shell (0.02023 vs 0.01986), and Gyroid pattern (0.02012 vs 0.01998).

Main-effects means showed small differences (**Figure 2**); significant three-way interactions (Infill×Shell×Pattern; Layer×Shell×Pattern) indicate multi-factor control of permeability (**Figure 3**).

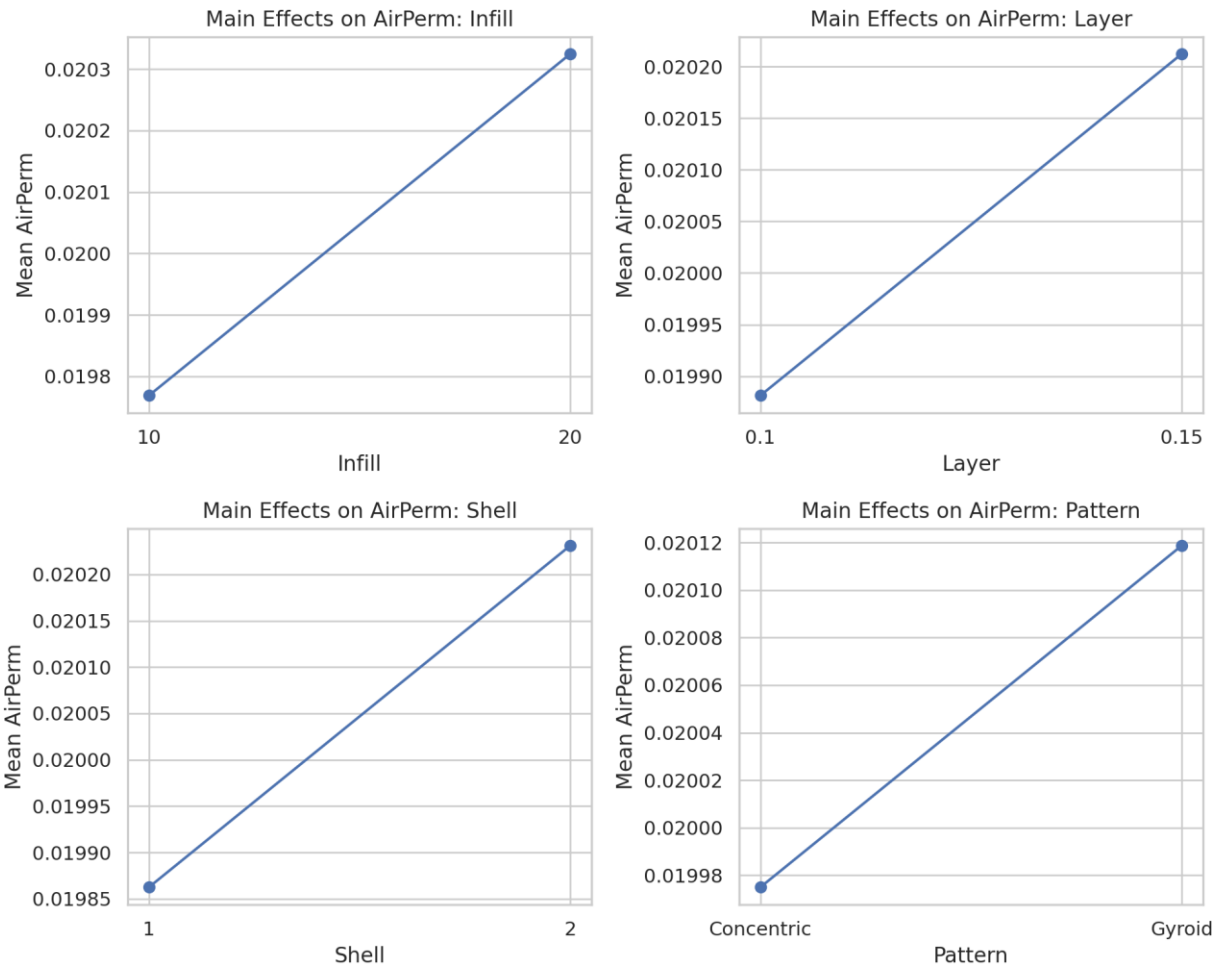

Figure 2. Main-effects plots for Air Permeability (Stage-1 Burnout).

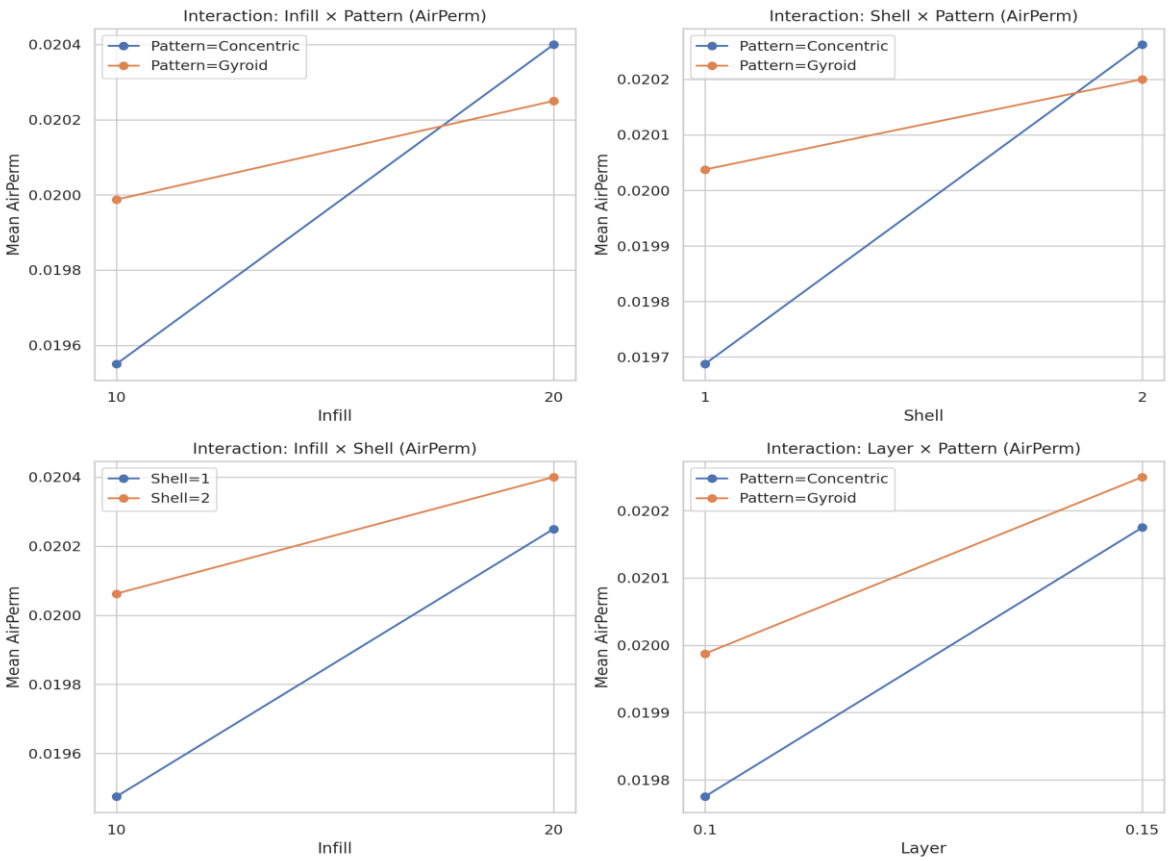

Figure 3. Interaction plots for Air Permeability (Stage-1 Burnout).

Dye Penetrant Indication (Stage-2, up to 650 °C)

Dye readings increased sharply with shell thickness and moderately with layer height (**Figure 4**); several interactions were highly significant, confirming combined factor effects (**Figure 5**).

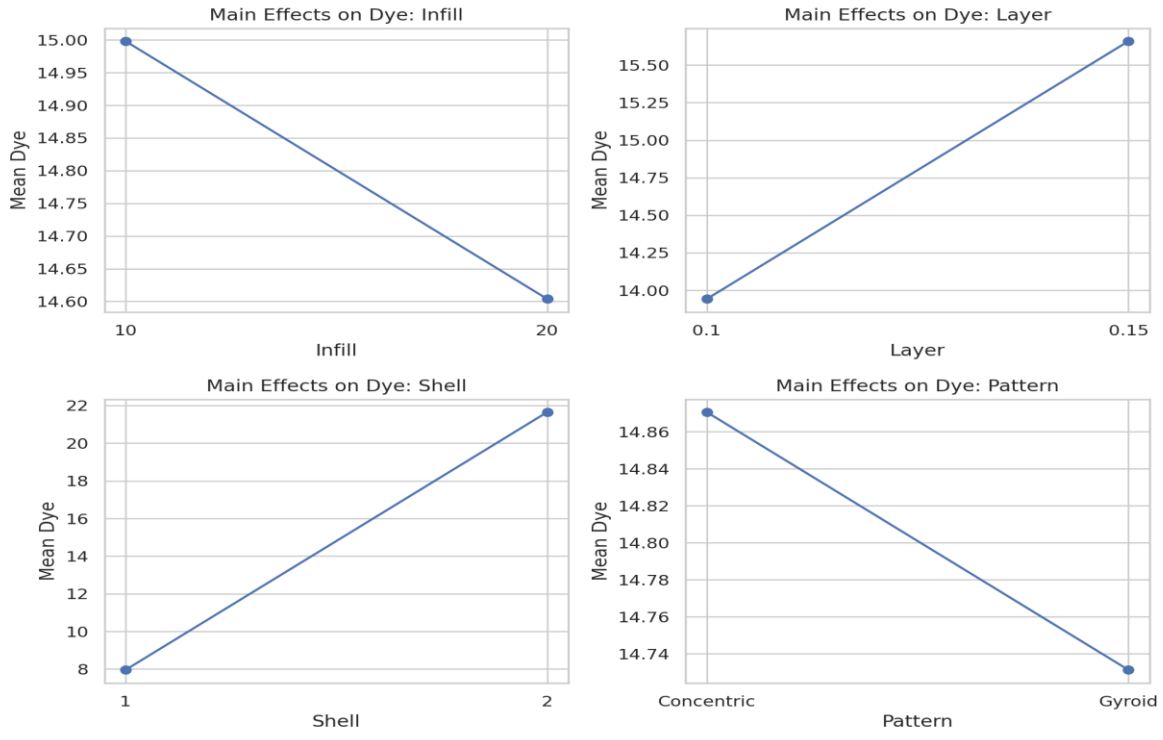

Figure 4. Main-effects plots for Dye Penetrant Indication (Stage-2 Burnout).

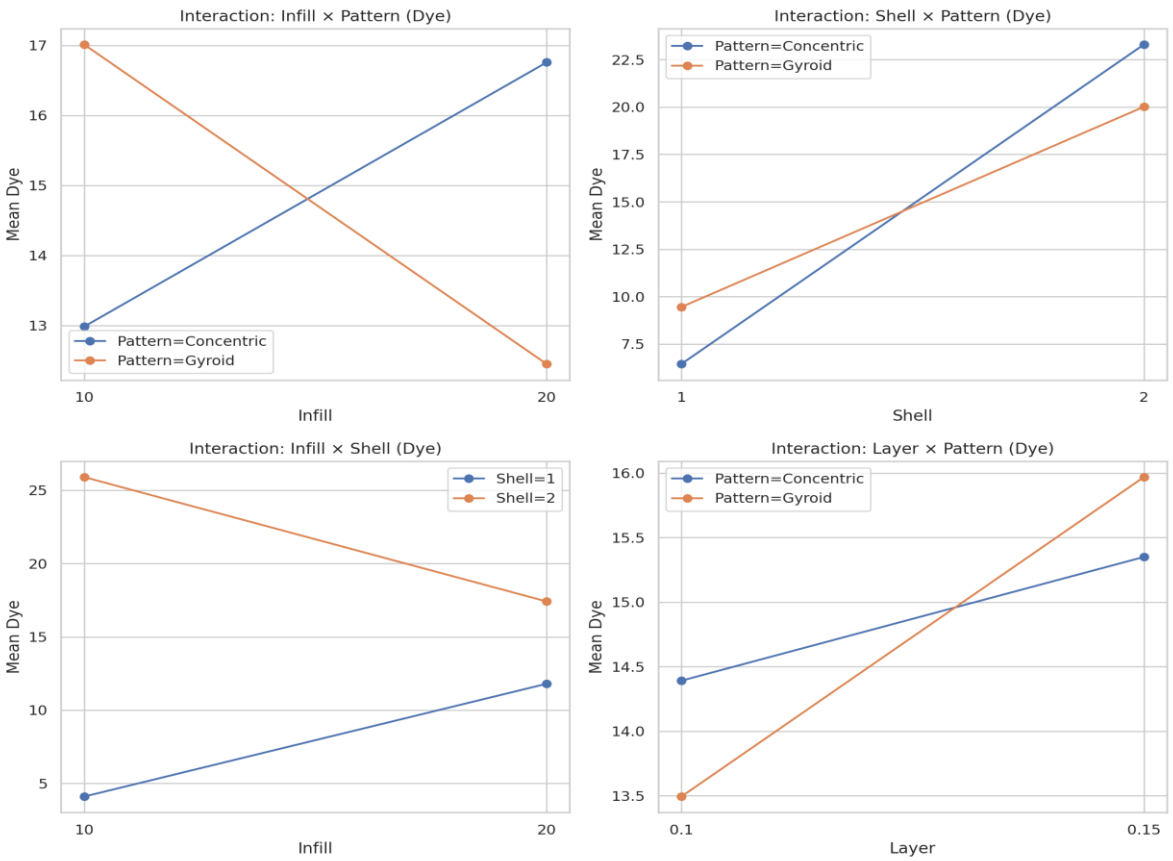

Figure 5. Interaction plots for Dye Penetrant Indication (Stage-2 Burnout).

Visual Cracking (binary)

Crack proportion was 100% at 2 mm shell versus 50% at 1 mm (Fisher exact p = 0.00245; Chi-square p = 0.00427). Other factors showed non-significant differences. Quasi-complete separation suggests exact tests over GLM.

Comprehensive ANOVA: Air Permeability (Type II)

No main effects reached significance ($p > 0.05$). Two three-way interactions were significant: Infill×Shell×Pattern ($F = 5.067$, $p = 0.03879$) and Layer×Shell×Pattern ($F = 6.975$, $p = 0.01779$) (Table 2). Practically, early-stage gas evacuation depends on combined settings of shell, pattern, and either infill or layer height; optimisation should evaluate these factors jointly. Residual diagnostics indicated non-normality (Shapiro–Wilk $p \approx 5.8\times10^{-7}$); a log transformation preserved the same interaction significance but did not restore normality (Shapiro–Wilk $p \approx 4.0\times10^{-7}$)

Table 2. Full ANOVA for Air Permeability (sum of squares, F, and p-values).

Term	Sum Sq	F	p-value
C(Infill)	0.000002	2.489	0.13424
C(Layer)	0.000001	0.883	0.36148
C(Shell)	0.000001	1.094	0.31121
C(Pattern)	0.000000	0.166	0.68892

C(Infill):C(Layer)	0.000002	2.270	0.15140
C(Infill):C(Shell)	0.000000	0.385	0.54375
C(Layer):C(Shell)	0.000000	0.071	0.79373
C(Infill):C(Pattern)	0.000001	0.694	0.41707
C(Layer):C(Pattern)	0.000000	0.038	0.84787
C(Shell):C(Pattern)	0.000000	0.342	0.56676
C(Infill):C(Layer):C(Shell)	0.000000	0.196	0.66361
C(Infill):C(Layer):C(Pattern)	0.000001	0.817	0.37942
C(Infill):C(Shell):C(Pattern)	0.000005	5.067	0.03879
C(Layer):C(Shell):C(Pattern)	0.000007	6.975	0.01779
C(Infill):C(Layer):C(Shell):C(Pattern)	0.000001	0.636	0.43677
Residual	0.000016	—	—

Comprehensive ANOVA: Dye Penetrant (Type II)

Shell thickness is the dominant main effect ($F = 2135.9$, $p \approx 1.84e\text{-}18$), with Layer height also significant ($F = 33.55$, $p \approx 2.75e\text{-}05$). Several interactions (Infill×Shell, Infill×Pattern, Shell×Pattern, Infill×Layer×Shell) are highly significant, confirming that thicker shells amplify defect severity under certain infill-pattern and layer combinations (Table 3). Operationally, lowering shell thickness and controlling the interacting settings reduces Stage-2 surface indications.

Table 3. Full ANOVA for Dye Penetrant Indication (sum of squares, F, and p-values).

Term	Sum Sq	F	p-value
C(Infill)	1.244	1.770	2.020e-01
C(Layer)	23.581	33.547	2.752e-05
C(Shell)	1501.383	2135.898	1.840e-18
C(Pattern)	0.155	0.221	6.446e-01
C(Infill):C(Layer)	11.127	15.830	1.079e-03
C(Infill):C(Shell)	523.180	744.287	7.627e-15
C(Layer):C(Shell)	19.924	28.344	6.851e-05
C(Infill):C(Pattern)	138.819	197.487	2.023e-10
C(Layer):C(Pattern)	4.598	6.541	2.108e-02
C(Shell):C(Pattern)	79.097	112.525	1.201e-08

C(Infill):C(Layer):C(Shell)	263.064	374.241	1.598e-12
C(Infill):C(Layer):C(Pattern)	63.253	89.985	5.694e-08
C(Infill):C(Shell):C(Pattern)	2.779	3.953	6.417e-02
C(Layer):C(Shell):C(Pattern)	83.754	119.150	8.011e-09
C(Infill):C(Layer):C(Shell):C(Pattern)	126.683	180.222	3.985e-10
Residual	11.247	—	—

CONCLUSION

Shell thickness is the primary lever for Stage-2 defects; 1 mm shells reduce dye and cracking versus 2 mm. Stage-1 permeability is controlled by higher-order interactions—avoid single-factor tuning. Pattern should be tuned jointly with shell, infill and layer height due to strong interactions. The two-stage burnout workflow enables early identification of sensitive combinations and robust Stage-2 inference via exact tests.

ACKNOWLEDGEMENT

The authors would like to thank the Faculty of Industrial and Manufacturing Technology and Engineering at Universiti Teknikal Malaysia Melaka (UTeM) for financial, educational, and technical support throughout this research.

REFERENCES

1. Campbell, J. (2015). Complete casting handbook: Metal casting processes, metallurgy, techniques and design (2nd ed.). Elsevier. https://doi.org/10.1016/C2013-0-16361-1
2. Abisuga, O. A., Doran, K., & de Beer, D. (2022). Study of investment casting process for 3D printed jewellery design. MATEC Web of Conferences, 370, 04002. https://doi.org/10.1051/matecconf/202237004002
3. Jones, S., & Yuan, C. (2003). Advances in shell moulding for investment casting. Journal of Materials Processing Technology, 135(2–3), 258–265. https://doi.org/10.1016/S0924-0136(02)00828-1
4. Hague, R., Campbell, I., & Dickens, P. (2003). Implications on design of rapid manufacturing. Proc. IMechE Part C: J. Mech. Eng. Sci., 217(1), 25–30. https://doi.org/10.1243/095440603762554587
5. Chhabra, M., & Singh, R. (2011). Rapid casting solutions: A review. Rapid Prototyping Journal, 17(5), 328–350. https://doi.org/10.1108/13552541111156469
6. Snelling, D., Li, Q., Meisel, N., Williams, C., & Batra, R. (2015). The effects of 3D printed molds on metal casting. Journal of Manufacturing Processes, 19, 1–7. https://doi.org/10.1016/j.jmapro.2015.05.002
7. Ngo, T. D., Kashani, A., Imbalzano, G., Nguyen, K. T. Q., & Hui, D. (2018). Additive manufacturing (3D printing): A review of materials, methods, applications and challenges. Composites Part B: Engineering, 143, 172–196. https://doi.org/10.1016/j.compositesb.2018.02.012
8. Bassoli, E., Gatto, A., Iuliano, L., & Violante, M. G. (2007). 3D printing technique applied to rapid casting. Rapid Prototyping Journal, 13(3), 148–155. https://doi.org/10.1108/13552540710750898
9. Singh, R., & Sachdeva, A. (2011). Optimization of investment casting process parameters using DOE. Journal of Manufacturing Technology Management, 22(4), 468–484. https://doi.org/10.1108/17410381111126401
10. Kumar, S., & Kruth, J. P. (2010). Composites by rapid prototyping technology. Materials & Design, 31(2), 850–856. https://doi.org/10.1016/j.matdes.2009.06.045
11. Yarlagadda, P. K. D. V., & Cheng, C. K. (2001). Thermal stresses in investment casting shells. Journal of Materials Processing Technology, 110(1), 1–8. https://doi.org/10.1016/S0924-0136(00)00804-6

12. Ding, D., Pan, Z., Cuiuri, D., & Li, H. (2015). Wire-feed additive manufacturing of metal components. International Journal of Advanced Manufacturing Technology, 81, 465–481. https://doi.org/10.1007/s00170-015-7077-3
13. Kumar, P., Ahuja, I. P. S., & Singh, R. (2012). Application of fusion deposition modelling for rapid investment casting. International Journal of Materials Engineering Innovation, 3(3), 204–221. https://doi.org/10.1504/IJMATEI.2012.050613
14. Ferreira, J. C., Mateus, A., & Alves, N. (2007). Rapid tooling aided by reverse engineering. Journal of Materials Processing Technology, 183(2–3), 412–419. https://doi.org/10.1016/j.jmatprotec.2006.10.026
15. Zhang, Y., Chou, K., & He, Y. (2016). Numerical investigation of gas escape in investment casting shells. Journal of Manufacturing Science and Engineering, 138(11), 111005. https://doi.org/10.1115/1.4033865
16. Bassoli, E., Atzeni, E., Salmi, A., & Calignano, F. (2018). Additive manufacturing for investment casting applications. Procedia CIRP, 70, 3–8. https://doi.org/10.1016/j.procir.2018.02.014
17. Singh, S., Ramakrishna, S., & Berto, F. (2020). 3D printing of polymer composites. Composites Part B: Engineering, 191, 107938. https://doi.org/10.1016/j.compositesb.2020.107938
18. ASTM E1417/E1417M-16 (2016). Standard practice for liquid penetrant testing. ASTM International. https://doi.org/10.1520/E1417_E1417M-16
19. Gibson, I., Rosen, D., & Stucker, B. (2015). Additive manufacturing technologies (2nd ed.). Springer. https://doi.org/10.1007/978-1-4939-2113-3
20. Kalpakjian, S., & Schmid, S. (2014). Manufacturing engineering and technology (7th ed.). Pearson Education.